(Received 14 September 2023, Accepted 1 December 2023, Scheduled 14 December 2023)

An Ultra-Wideband MIMO Antenna Based on Dual-Mode Transmission Line Feeding for Wireless Communication

Xianjing Lin[1], Gengtao Huang[1], and Yao Zhang[2,*]

[1]School of Electronic Engineering and Intelligence, Dongguan University of Technology, Dongguan, Guangdong 523808, China
[2]Institute of Electromagnetics and Acoustics, Xiamen University, Xiamen, Fujian 361005, China

ABSTRACT: An ultra-wideband (UWB) MIMO antenna based on dual mode transmission line feeding for wireless communication is proposed in this article. The general method of realizing a UWB MIMO antenna is using different shapes of monopoles acting as a MIMO antenna element, while the ultra-wideband character of the proposed MIMO antenna is mainly obtained by the use of a dual-mode transmission line in the coplanar waveguide (CPW) feeding line, which offers a novel method. The proposed MIMO antenna element is a rose-shaped monopole fed by a CPW feeding line. Compared to the traditional monopole, a rose-shaped monopole can introduce several extra resonant frequencies, and the impedance bandwidth can be improved. Besides, a dual-mode transmission line (DMTL) is introduced by adding specific stubs to the CPW feeding line. Arranging the stubs at the half wavelengths of the desired frequencies, mode transformation can be accomplished, and additional resonant modes can be generated. As a result, the impedance bandwidth can be further broadened. Results show that the fractional impedance bandwidth of the proposed UWB antenna element is 165.5% (2.59 GHz to 26.61 GHz). Then, the UWB antenna is applied to design a 4-element MIMO antenna. By loading four u-typed decoupling structures at the center of the MIMO antenna, the port-to-port isolation of the MIMO antenna can be increased to 20 dB within a wide bandwidth, especially 25.3 dB at the higher band (14–25 GHz). The proposed UWB MIMO antenna is manufactured and tested. Experimental results show that the impedance bandwidth covers 2.40 GHz to 25 GHz (165%). The diversity gain (DG) of the antenna in the operating band is about 10; the envelope correlation coefficient (ECC) is less than 0.002; and the radiation efficiency ranges from 85% to 95% in the whole working band. The design is a preferable candidate for MIMO systems.

1. INTRODUCTION

Ultra-wideband (UWB) technology is widely used in various fields such as detection imaging, missile and radar systems, as UWB technology has the advantages of high transmission rate, strong penetration, multipath resolution, and low power consumption [1, 2]. Applying UWB antennas to modern wireless communication system will have great application value. It is also an ideal choice to realize the miniaturization, integration, and improvement of the data transmission rate and channel capacity of communication equipment. However, UWB antennas often suffer from the difficulty of long-range transmission due to its low spectral density [3]. Multi-input multi-output (MIMO) technology can effectively improve this shortcoming. MIMO technology uses multiple antenna elements at the transmitter and receiver at the same time, and the diversity technology can improve the communication capacity and effectively avoid multipath effect. In recent years, researchers around the world have combined UWB technology and MIMO technology to develop UWB-MIMO systems. UWB-MIMO technology can effectively improve the wireless communication capacity, rate and suppress the multipath effect [4].

Recently, a number of UWB MIMO antennas have been reported [5–17]. In [5], a 4-element UWB MIMO antenna employing two orthogonally placed substrates was proposed, and the antenna operated from 2 to 12 GHz with an isolation of 17 dB and large ECC value. L-type and Z-type 4-element MIMO antennas with separate ground were proposed [6]. The size of the antenna was large, which occupied $150 \times 75\,\text{mm}^2$ ($3.57\lambda g \times 1.79\lambda g$, λg is the waveguide wavelength of the lowest frequency), and the bandwidths and isolation were limited. An 8-element MIMO antenna with the same size of [6] using two small dielectric substrates perpendicular to the main substrate was presented [7]. The isolation was better than 20 dB, but the efficiency was only 47%, and the ECC was very high. In [8], a 4-element wideband high gain MIMO antenna was proposed. The operating frequency band ranged from 2 to 6 GHz, and the peak gain of the antenna was above 4.8 dBi, but the antenna suffered from large size and poor isolation. A 2-element UWB MIMO antenna with a planar decoupling structure was presented in [9], and the size of the antenna was $93 \times 47\,\text{mm}^2$ ($2.02\lambda g \times 1.02\lambda g$). It covered the band from 3.1 to 10.6 GHz, and the ports isolation was above 31 dB. However, the ECC was also high. MIMO antennas with notched band were reported in [10–12]. They were inapplicable to ultra-wideband full band communication. In [13], a UWB (4-element) MIMO antenna with a compact size of $56 \times 68\,\text{mm}^2$ ($1.53\lambda g \times 1.85\lambda g$) was proposed, and the impedance bandwidth reached 125.83% (3.89–17.09 GHz). However, the isolation within the working band is only 15 dB. In [14], a compact (4-element) MIMO antenna with size of $60 \times 60\,\text{mm}^2$ ($1.26\lambda g \times 1.26\lambda g$) based on a coplanar waveguide feeding was proposed. The impedance band covered 3 to 11 GHz (114.28%), and the isolation was more than

* Corresponding author: Yao Zhang (zhangsantu@xmu.edu.cn).

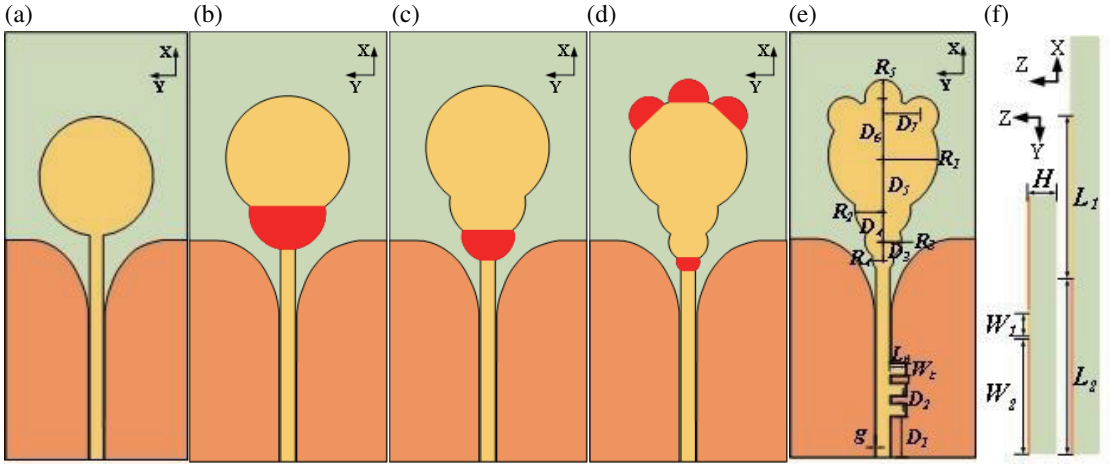

FIGURE 1. The evolution of the antenna element. (a) antenna I. (b) antenna II. (c) antenna III. (d) antenna IV. (e) antenna V. (f) antenna VI.

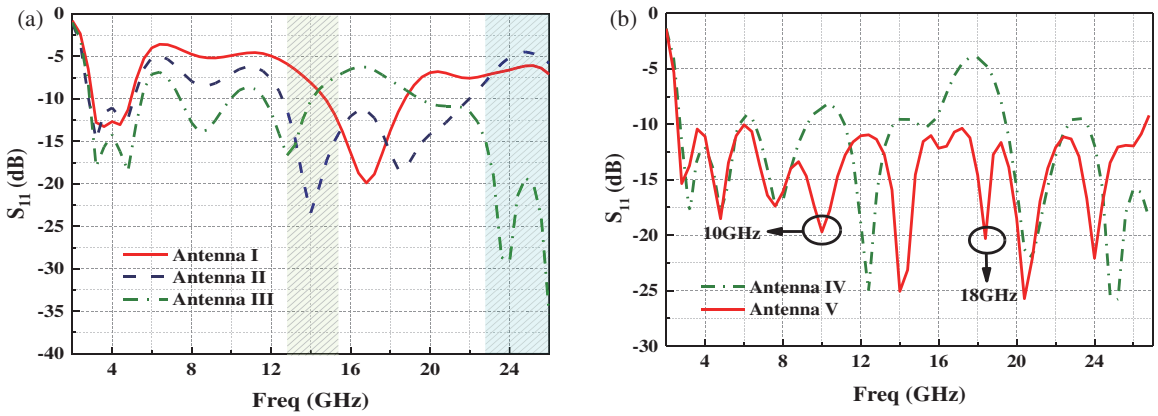

FIGURE 2. The reflection coefficients of the five antennas. (a) antenna I, II and III. (b) antenna IV and V.

20 dB. In general, the above-mentioned UWB-MIMO antennas cannot simultaneously realize wide bandwidth, high isolation, and compact size.

In this paper, a 4-element UWB MIMO antenna based on dual-mode transmission line feeding is proposed. The element radiator of the proposed UWB MIMO antenna is designed to be a rose-shaped monopole. Unlike traditional monopole, the rose-shaped monopole consists of four cascading different diameter circular patches and three arc-shaped patches loaded onto the largest circular patch. This design can extend antenna surface current path to obtain compact size and generate multiple resonating frequencies. Moreover, by loading stubs to the CPW feeding line, the DMTL can be obtained. Thus, the required resonant frequency can be introduced to further increase the impedance bandwidth. Simulation results show that the impedance bandwidth of the element is 165% (2.40–25 GHz). Then, a 4-element MIMO antenna based on this element is developed. By loading four u-typed decoupling structures at the center of the MIMO antenna, the isolation of the MIMO antenna is increased to 20 dB, especially 25.3 dB at the higher band (14–25 GHz). And the envelope correlation coefficient is less than 0.002; the diversity gain is about 10 dB; and the radiation efficiency is above 88.9%. Above all, the antenna possesses satisfactory MIMO performances.

2. ANALYSIS AND DESIGN OF THE UWB ANTENNA ELEMENT

The evolution of the UWB antenna element is shown in Fig. 1, and the corresponding simulated reflection coefficients are drawn in Fig. 2. The element is printed on Rogers 4003 ($\varepsilon_r = 3.55$, $\tan\delta = 0.0027$) with a thickness 0.508 mm, and the size is $45 \times 20\,\text{mm}^2$. The optimized parameters are listed in Table 1. It can be seen that Antenna I is a CPW-fed circular monopole antenna, and six resonating frequencies can be excited from 3 to 25 GHz. The initial size of the monopole antenna is designed at a quarter wavelength of 3.6 GHz. Antenna II and Antenna III are cascaded with circular patches of different sizes under the original monopole antenna, and they can increase current paths so as to generate two more resonating frequencies. The same technology is applied to Antenna IV, and two more resonating frequencies are generated. Although the resonating frequencies are increased in Antenna IV, the impedance matching is not good at 10 and 18 GHz, and thus Antenna IV cannot be a

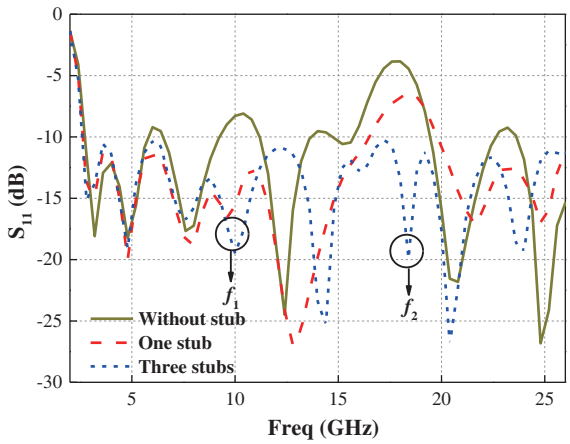

FIGURE 3. S_{11} of the antenna V with one stub, three stubs and without stub.

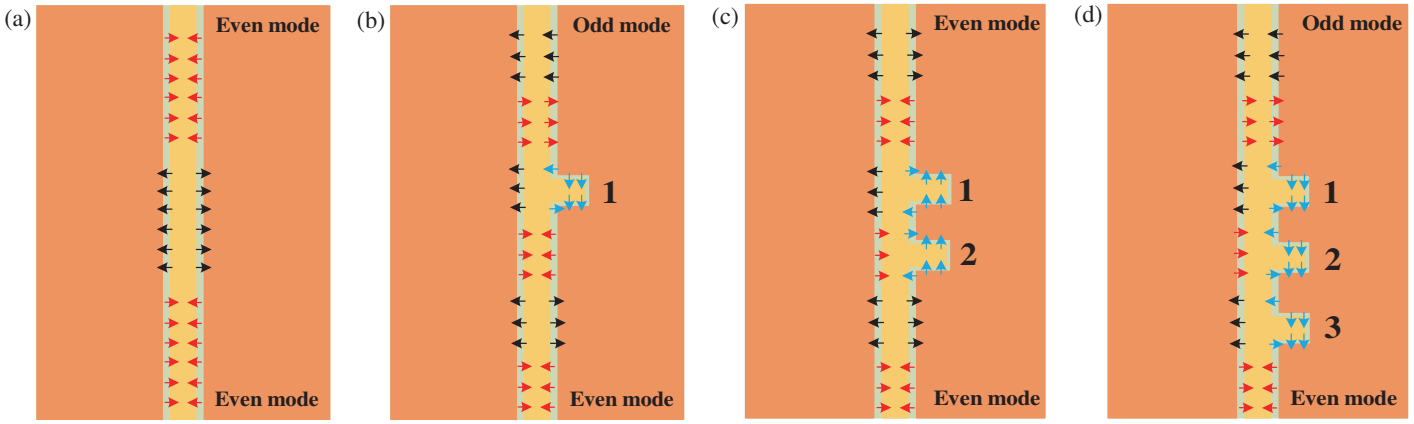

FIGURE 4. Electric field distribution of the CPW feeding line, (a) without the stubs, (b) with stub 1, (c) with stubs 1 and 2, (d) with stubs 1, 2, and 3.

wideband antenna. Consequently, Antenna V is designed using a dual-mode transmission line (DMTL) fed monopole antenna based on Antenna IV. By loading three open-ended stubs at the CPW feeding line, mode transformation can be realized. Thus, 10 and 18 GHz resonating frequencies can be introduced in Antenna V. Finally, Antenna V can cover 2.59 to 26.61 GHz (165.52%) and realize wideband performance. It should be mentioned that the CPW feeding technology is employed as it has the advantages of simple fabrication, strong flexibility, easy integration, compact size, and enhanced radiation performance compared to traditional microstrip transmission lines feeding [18]. The detailed working mechanism of the DMTL is analyzed as follows. Fig. 4 illustrates the ideal electric field distribution of the traditional CPW feeding transformed to dual-mode transmission feeding. As shown in Fig. 4(a), the CPW feeding structure consists of the central conductor and bilateral ground planes. The electric field is directed from the central conductor to the bilateral ground planes or inverse, which are represented in black and red arrows. In this case, the CPW feeding line is excited in the even mode. It should be noted that the black and red arrows represent the direction of the electric field passed by $1/2\lambda g$ transmission line. When one open-ended stubs are loaded at the right side of the central conductor, the direction of the electric field between the central conductor and the ground plane in the right is changed, as shown in Fig. 4(b). Thus, the CPW feeding line is excited from even mode to the odd one [19–21]. A new resonating frequency can be introduced. While two open-ended stubs are loaded in Fig. 4(c), the direction of the electric field between the central conductor and the ground plane in the right is changed twice, thereby, the CPW feeding line keeps even mode excited, and a new resonating frequency will not be created. If three open-ended stubs are loaded in Fig. 4(d), the mode transformation is still realized. Meanwhile, two extra resonating frequencies can be obtained. Fig. 5 shows the simulated electric field distribution of Antenna V. As predicted, the even mode is excited when no stubs are loaded at the CPW feeding line, or two stubs are loaded. While stub 1 is loaded at the $1/2\lambda$g of 10 GHz away from the port, stub 3 at the $1/2\lambda g$ of 19 GHz, and stub 2 at the center of stub 1 and stub 3, the dual mode feeding line is accomplished. And the 10 GHz and 19 GHz resonating frequencies are introduced, as seen in Fig. 2(b). The reflection coefficient of Antenna V with one stub, three stubs and without stub can also verify the opinion. It can be seen in Fig. 3 that one increased resonator frequency is generated at f_1 (about 10 GHz), when one stub is loaded at 8.2 mm away from the feeding port. Two increased

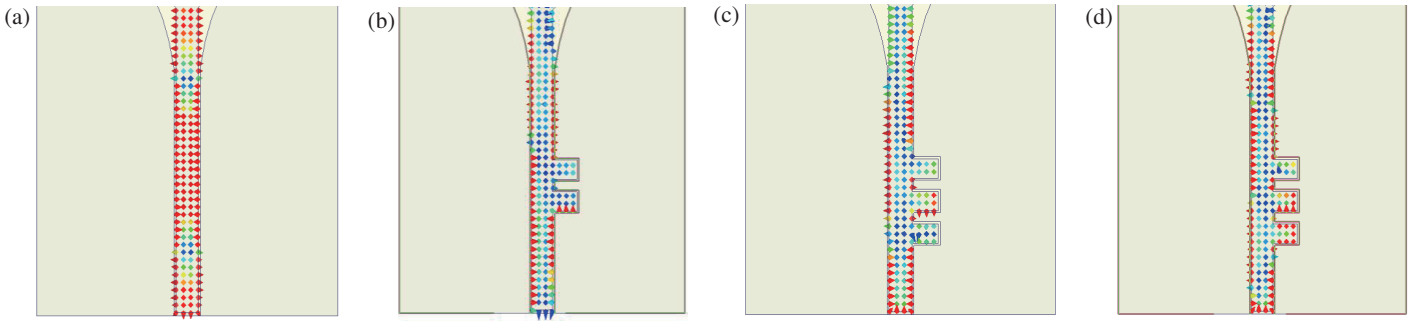

FIGURE 5. Simulated electric field distribution of the CPW feeding line, (a) without stubs at 10 GHz, (b) with two stubs at 10 GHz, (c) with three stubs at 10 GHz, (d) with three stubs at 18 GHz.

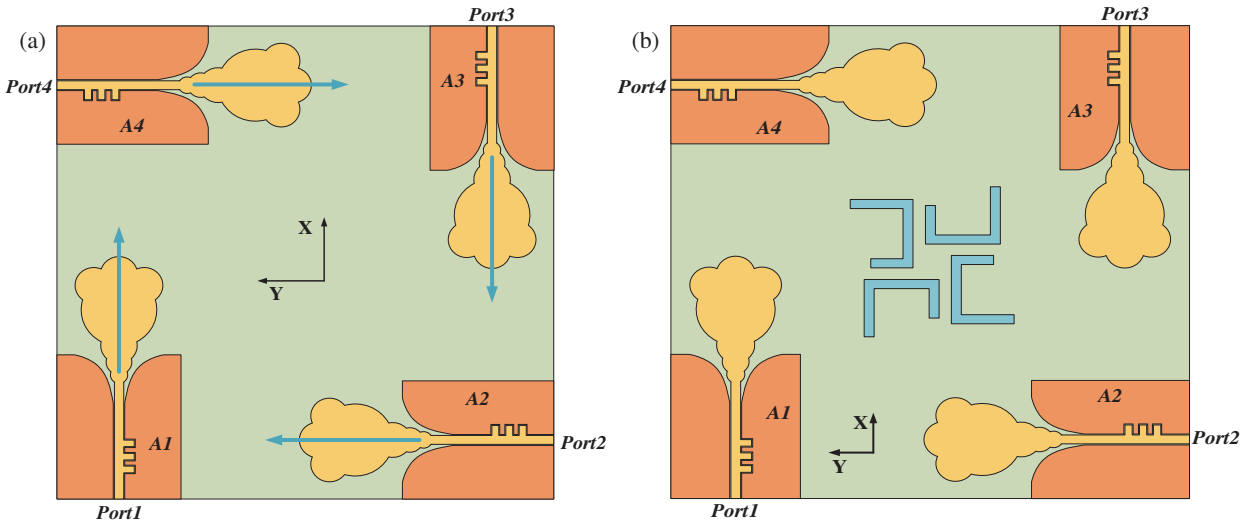

FIGURE 6. The 4-element UWB-MIMO antenna, (a) without the decoupling structure, (b) with the decoupling structure.

resonator frequencies are generated at f_1 (about 10 GHz) and f_2 (about 19 GHz) compared to the antenna element without stub, when the first stub is loaded at 8.2 mm, and the third stub is loaded at 4.2 mm away from the feeding port. The distances of 8.2 mm and 4.2 mm are about half wave-guide wavelengths of 10 GHz and 19 GHz.

Based on the above method, a design guideline of the proposed UWB-MIMO antenna element with dual-mode transmission line feeding can be summarized as below:

(1) Step 1: design a CPW fed circular monopole antenna.

(2) Step 2: modify the monopole to a gradient one, which can improve the broadband impedance matching condition.

(3) Step 3: employ several small circular patches at the edge of the gradient circular monopole to increase more current paths so as to generate extra resonating frequencies.

(4) Step 4: load odd numbered open-ended stubs at the CPW feeding line to realize mode transformation, which can introduce required resonating frequencies to further improve the impedance matching. And ultra-wide band operation can be thus realized.

3. ANALYSIS AND DESIGN OF THE MIMO ARRAY

3.1. UWB-MIMO Antenna without Decoupling Structure

Based on the UWB antenna element in Section 2, a 4-element UWB-MIMO antenna is constructed, which is shown in Fig. 6(a). The UWB-MIMO antenna elements are orthogonal to each other [22–25]. At this time, the antenna elements in positive cross-polarization can only sense weak signals. The details are as follows: polarization directions of each element are represented by the blue arrows. Elements A1 and A3 are linear polarization in the x direction, while A2 and A4 are linear polarization in the y direction. The intrinsic polarization isolation can ensure a low coupling between the elements of x and y polarization direction. However, the elements in the same polarization direction (A1, A3 and A2, A4) are seriously interfered to each other.

3.2. UWB-MIMO Antenna with Decoupling Structure

To improve the isolation of the UWB-MIMO antenna, the decoupled structure is introduced, as shown in Fig. 6(b). The decoupling structure is composed of four U-shaped metal strips, and they are arranged at the center of the MIMO antenna with

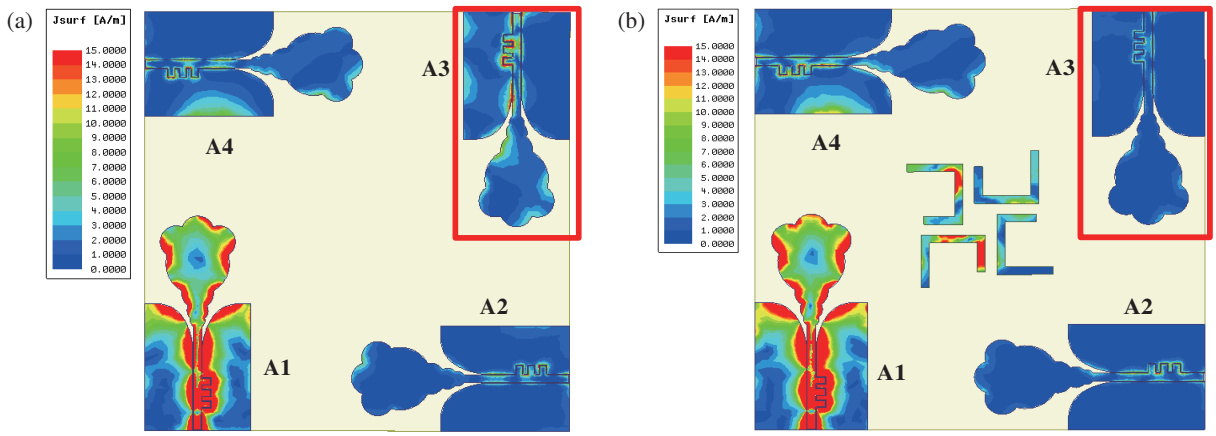

FIGURE 7. Current distributions of the MIMO antenna at 14 GHz with element A1 excited, (a) without the decoupling structure, (b) with the decoupling structure.

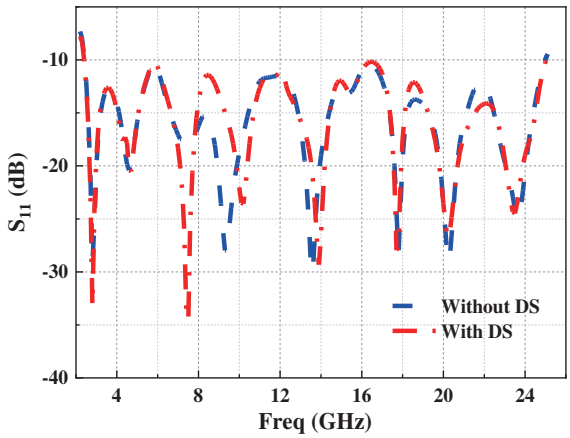

FIGURE 8. The S_{11} of the MIMO antenna with and without the decoupling structure (DS).

TABLE 1. Dimensions of the antenna (Unit: mm).

W_g	L_g	W_1	L_1	H	W	W_t	L_t	w	L_2
9.13	23	1.5	15.87	0.508	80	1.2	1.7	1.5	10
L_3	L_4	g	R_1	R_2	R_3	R_4	R_5	D_1	D_2
11.5	7	0.12	6	3	2	1.2	2	4.28	0.56
D_3	D_4	D_5	D_6	D_7	D_8	D_9	D_{10}	D_{11}	
1.95	3.3	4.62	7.05	4	18.98	27	9.5	2	

90° rotated. The U-shaped metal strips create another coupling path between the antenna elements to cancel the original coupling current. And the isolation of the MIMO antenna is increased. The current distributions of the MIMO antenna with and without decoupled structure at 14 GHz are depicted in Fig. 7. As seen, when element A1 is excited without the decoupling structure, the coupling between elements A3 and A1 is strong and is weak between the vertical direction elements (A2, A4). Once the U-shaped decoupling structure is added, the mutual coupling between elements A1 and A3 is decreased obviously, which is because the U-shaped metal strips can offer reverse current to counteract the coupling current. Therefore, the isolation between A1 and A3 can be improved. The S parameters of the MIMO antenna with and without decoupled structure exhibited in Fig. 8 and Fig. 9 demonstrate the analysis. It can be concluded that the reflection coefficient is almost unaffected with/without the decoupling structure. And the isolation is increased to 20 dB at the lower band (2.40–14 GHz) and 25 dB at the higher band (14–25 GHz). It should be mentioned that the above analysis is based on independent ground, which will affect the normal operation of the whole communication system [26]. Therefore, a shared ground plane is needed. The actual structure of the antenna can be seen in Fig. 10, and the corresponding simulated results of the antenna

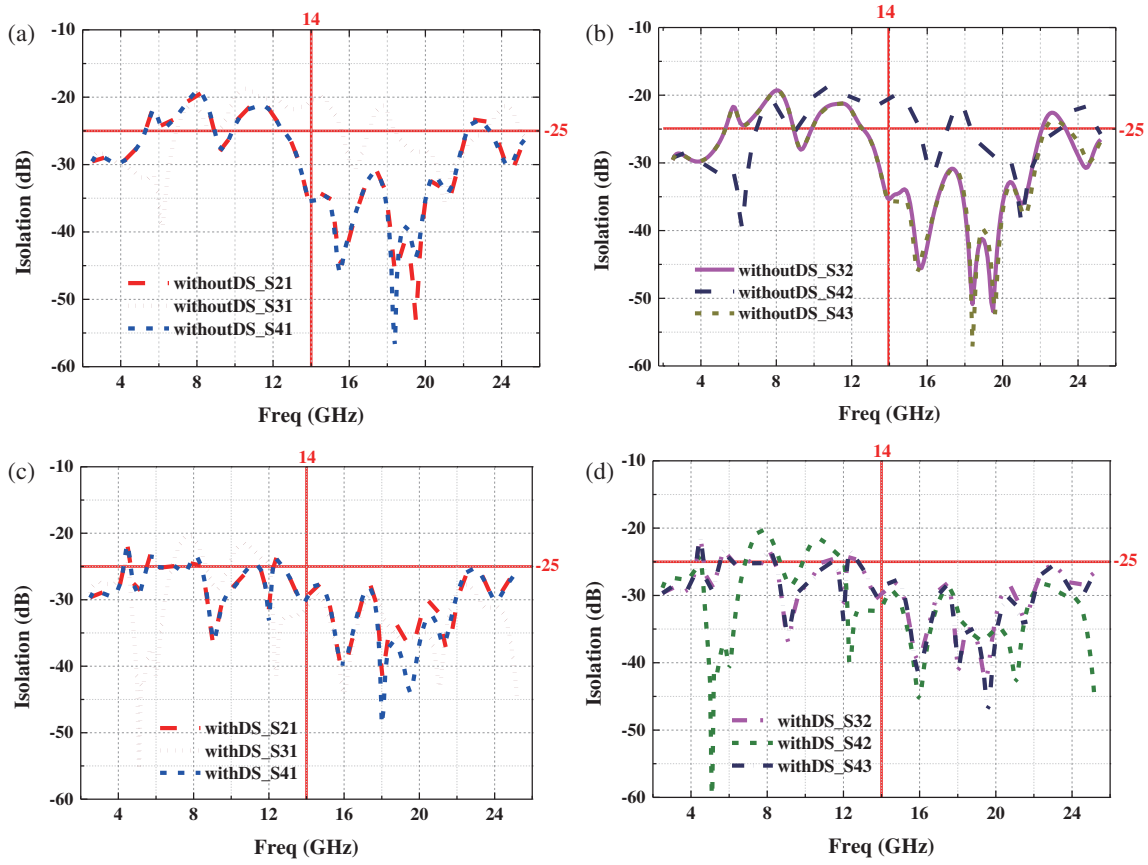

FIGURE 9. Simulation isolation of the MIMO antenna, (a) without the decoupling structure of S_{21}, S_{31} and S_{41}, (b) without the decoupling structure of S_{32}, S_{42} and S_{43}, (c) with the decoupling structure of S_{21}, S_{31} and S_{41}, (d) with the decoupling structure of S_{32}, S_{42} and S_{43}.

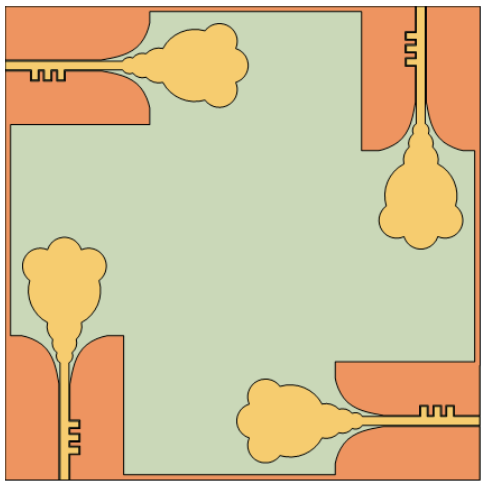

FIGURE 10. The 4-element UWB-MIMO antenna shared a ground plane.

are shown in Fig. 11. It can be seen that the impedance matching is slightly affected, and the isolation within the impedance matching bands is almost unaffected. The results show that the decoupling effect is mainly introduced by the decoupled structure and not by the separated ground.

4. MIMO ANTENNA IMPLEMENTATION AND MEASUREMENT RESULTS

4.1. Measured S-Parameters and Radiation Results

Figure 12 shows the fabrication prototype of the MIMO array antenna. For brevity, only the results of port 1 excited are

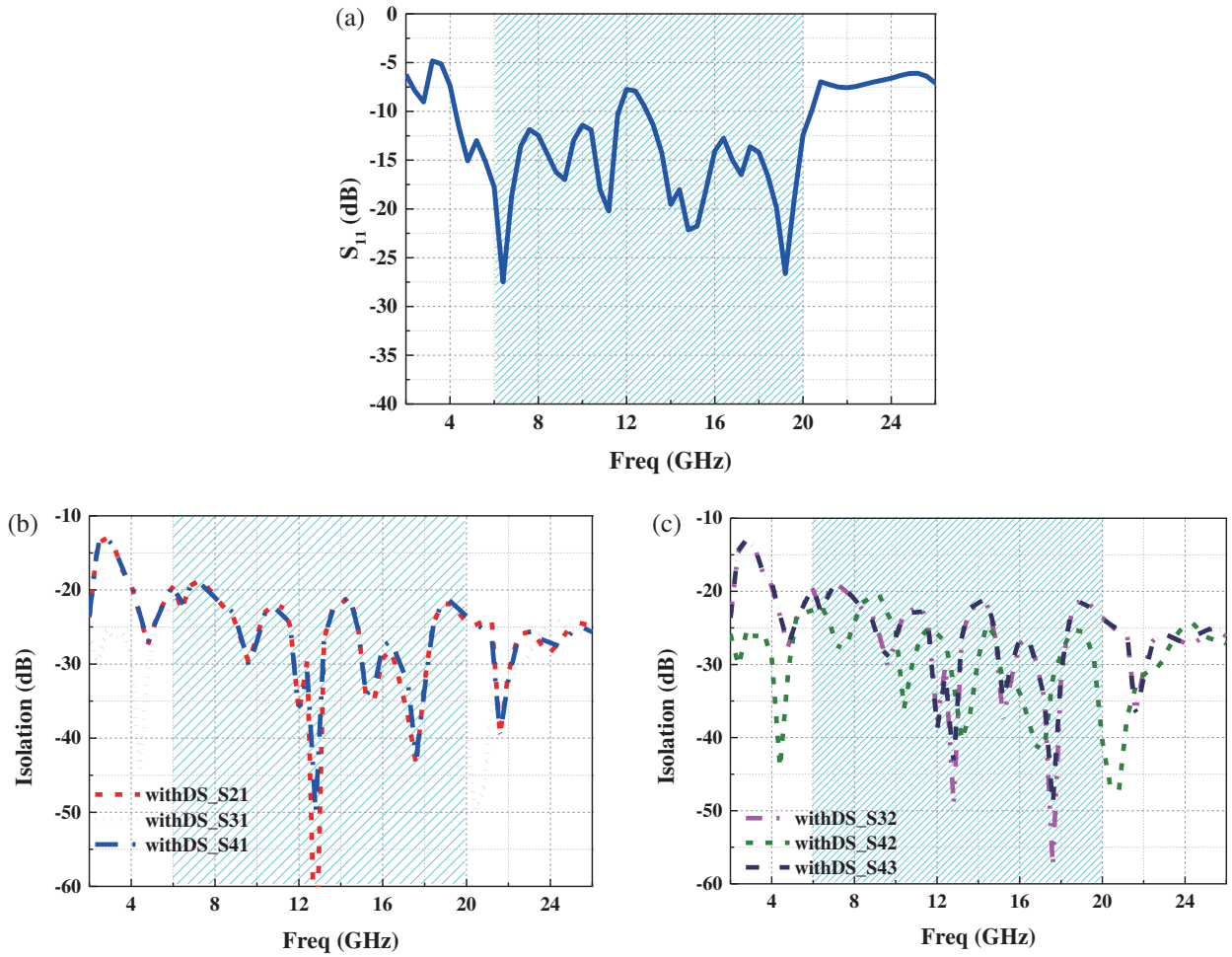

FIGURE 11. Simulated and measured S Parameters of the UWB-MIMO antenna shared a ground plane with the decoupling structure. (a) S_{11}. (b) S_{21}, S_{31} and S_{41}. (c) S_{32}, S_{42} and S_{43}.

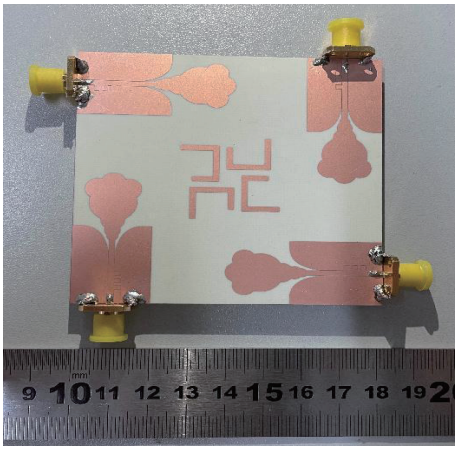

FIGURE 12. Fabricated prototype of the proposed antenna.

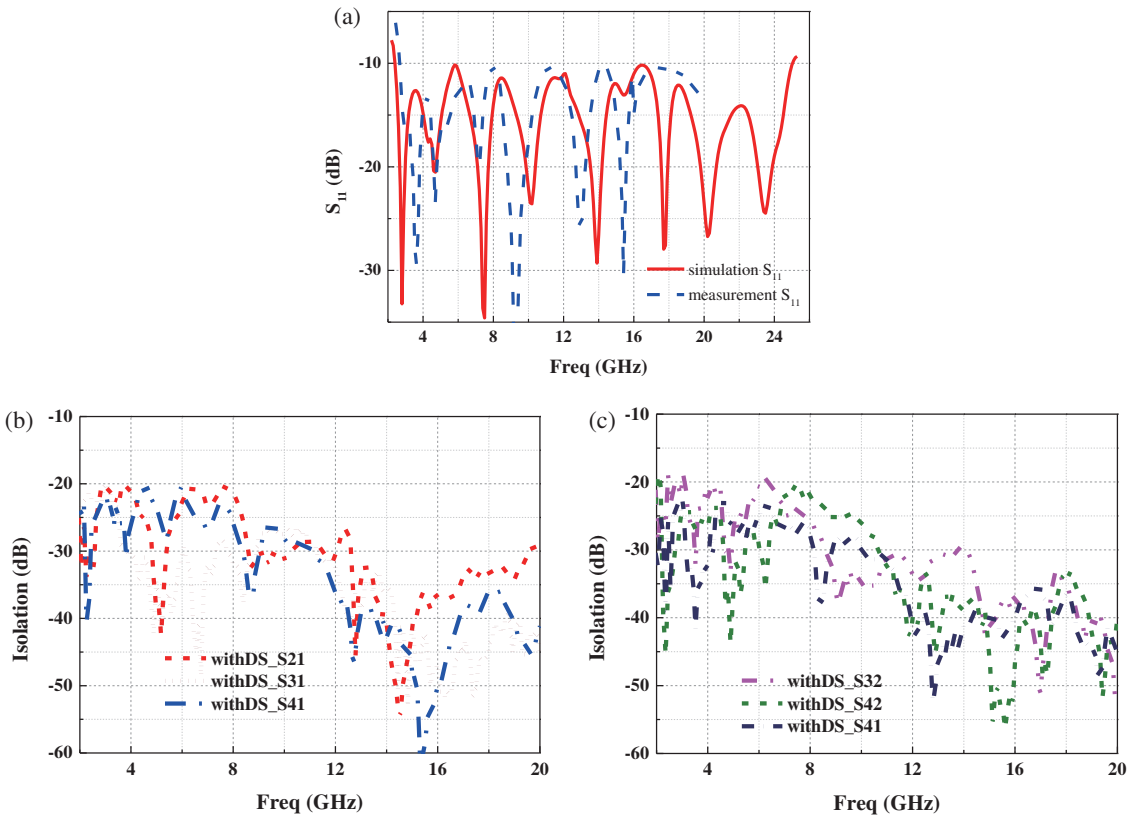

FIGURE 13. Simulated and measured S Parameters of the UWB-MIMO antenna. (a) S_{11}. (b) S_{21}, S_{31} and S_{41}. (c) S_{32}, S_{42} and S_{43}.

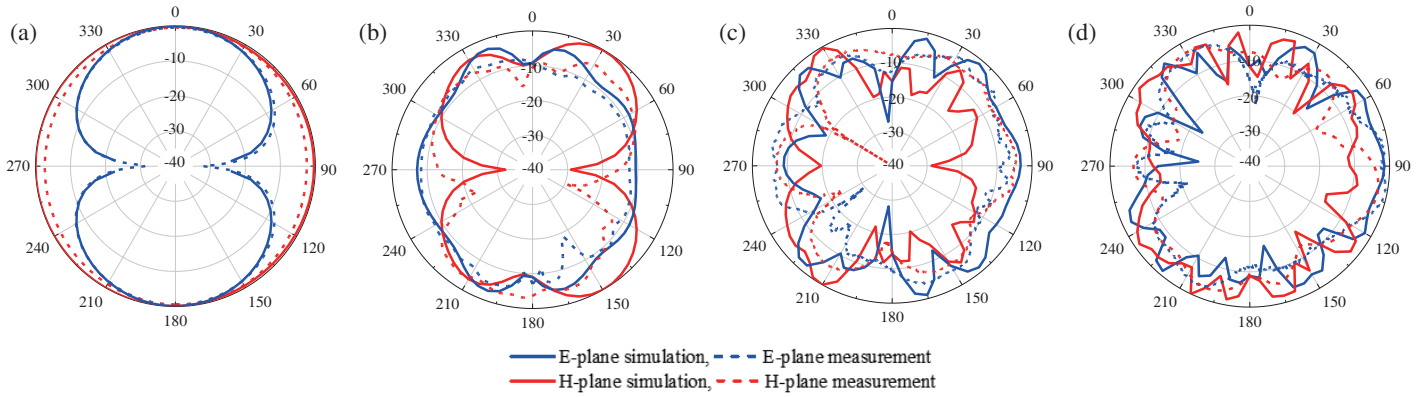

FIGURE 14. Radiation patterns at different frequencies. (a) 3 GHz. (b) 10 GHz. (c) 17 GHz. (d) 25 GHz.

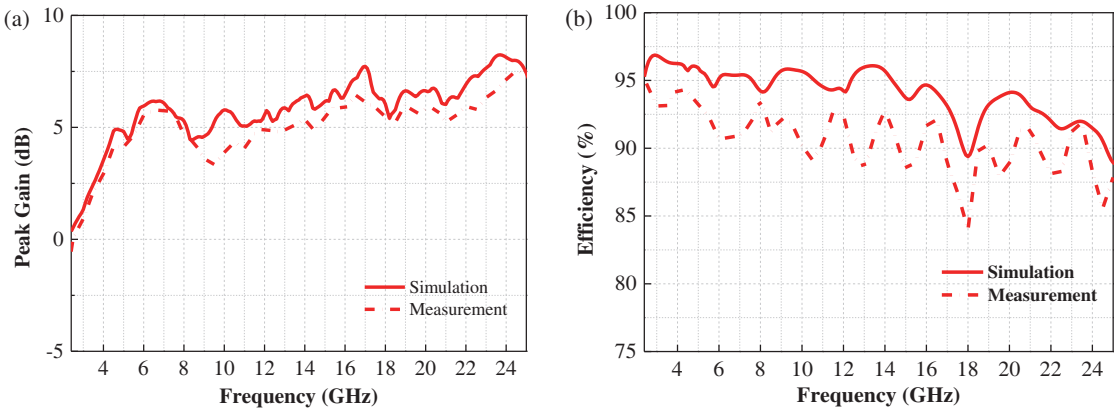

FIGURE 15. Peak gain and radiation efficiency of the UWB MIMO antenna, (a) peak gain, (b) radiation efficiency.

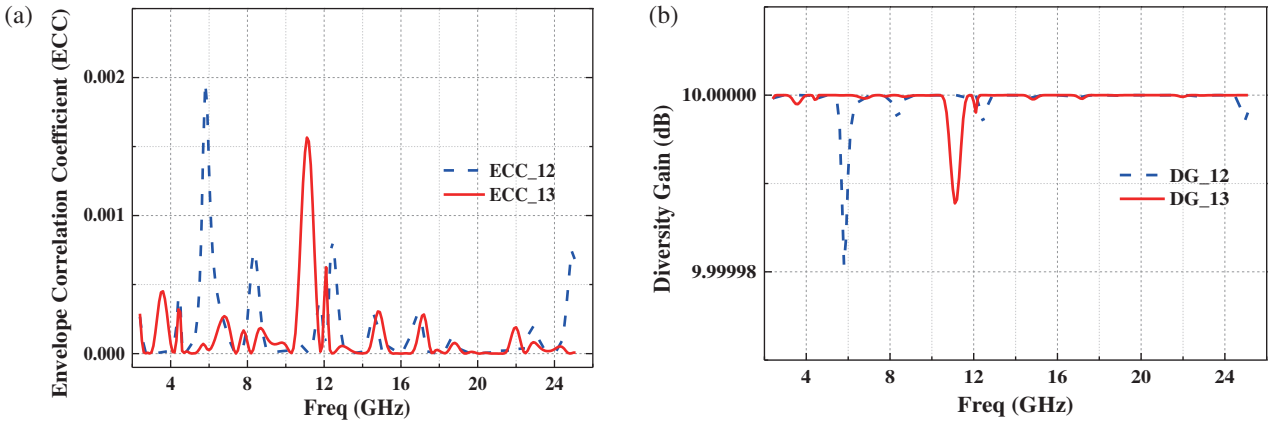

FIGURE 16. (a) ECC of the UWB MIMO antenna. (b) DG of the UWB MIMO antenna.

TABLE 2. Performance comparisons with the previously reported literature.

Ref.	size (mm^3)/λ^3	Number of elements	Frequency range (GHz)	Isolation (dB)	Peak gain (dBi)	Efficiency (%)	ECC
[5]	$50 \times 25 \times 1.6$ ($0.706 \times 0.353 \times 0.023$)	4	2–4.9 (84%) 6.4–12 (61%)	17	5.8	NG	0.15
[6]	$150 \times 75 \times 6.2$ ($3.57 \times 1.79 \times 0.15$)	4	3.4–3.6 (5.7%) 4.8–5 (4.1%)	16.5	5.1	85	0.01
[7]	$150 \times 75 \times 5.3$ ($3.57 \times 1.79 \times 0.15$)	8	3.4–3.6 (5.7%)	20	1.57	47	0.4
[8]	$80 \times 80 \times 1.57$ ($9.49 \times 9.49 \times 0.186$)	4	23–40 (54%)	20	12	70	0.0014
[9]	$93 \times 47 \times 1.6$ ($2.02 \times 1.02 \times 0.035$)	2	3.1–10.6 (109.49%)	31	3.5	70	0.2
[10]	$80 \times 80 \times 1.6$ ($1.176 \times 1.176 \times 0.024$)	4	2.1–3.3 (44.4%) 4.1–8.2 (66.7%) 8.6–20 (79.7%)	25	5.8	80	0.02
[11]	$50 \times 50 \times 1.6$ ($0.706 \times 0.706 \times 0.023$)	4	2–4.9 (84%) 6.4–12 (61%)	17.5	8.4	NG	0.15
[12]	$60 \times 60 \times 1.6$ ($0.6 \times 0.6 \times 0.016$)	4	3–4 (28.6%) 5.2–16.2 (102.8%)	17	5.9	65–91	0.3
[13]	$56 \times 82 \times 0.2$ ($1.52 \times 2.23 \times 0.005$)	4	3.89–17.09 (102.8%)	15	5.87	89	0.02
[14]	$60 \times 60 \times 1.6$ ($1.26 \times 1.26 \times 0.034$)	4	3–11 (114.3%)	20	3.4	68	0.02
This work	$80 \times 80 \times 0.508$ ($1.29 \times 1.29 \times 0.008$)	4	2.4–25 (165%)	20	7.38	85	0.002

presented since the elements are identical. Fig. 13 shows the measured and simulated S parameters of the proposed UWB-MIMO antenna when port 1 is excited and the other three ports terminated with 50 Ω load. The simulated and measured reflection coefficients of the proposed antenna are basically consistent except for some frequencies shift, because of the manufacturing and testing errors. It should be mentioned that only the measured S-parameters within 20 GHz of the proposed antenna are presented due to the limitation of N5227 Vector Network Analyzer. However, the measurement results agree well with the simulation ones within 20 GHz, indicating the correctness of the design method. As the coaxial feed transmission line has little influence on the result of the MIMO antenna, the simulation S_{11} of the MIMO antenna is obtained by the lump port excitation. The measured port-to-port isolation can reach about 20 dB in the whole operating band, especially 30 dB at the higher band (14–20 GHz). Fig. 14 shows the radiation patterns of the UWM MIMO antenna at 3 GHz, 10 GHz, 17 GHz, and 25 GHz. Omnidirectional radiation patterns as monopole are observed. As the radiation patterns at the higher frequencies are similar, the radiation pattern of 25 GHz is shown as an example. Fig. 15(a) depicts the peak gain curve of the antenna. The antenna has a gain between 0.9 and 7.38 dBi in the operating band. And the antenna radiation efficiency is above 85% as shown in Fig. 15(b).

4.2. Calculated Envelope Correlation Coefficient (ECC) and Diversity Gain (DG)

In MIMO antenna systems, it is hoped that the influence between antenna elements is small enough, and each element can work independently. The envelope correlation coefficient (ECC) is a physical quantity describing the correlation of signals between antenna elements. It is an important guiding evaluation for measuring the performance of MIMO antennas. Generally speaking, for a good MIMO antenna, the envelope correlation coefficient is less than 0.5. The value of the envelope correlation coefficient is smaller, and the independent performance of the antenna element is better. The following formula is used to calculate the envelope correlation coefficient [26]:

$$ECC = \frac{\left| \iint\limits_{4\pi} \left[E_1(\theta,\varphi) * E_2(\theta,\varphi)\, d\Omega \right] \right|^2}{\iint\limits_{4\pi} \left| E_1(\theta,\varphi) \right|^2 d\Omega \iint\limits_{4\pi} \left| E_2(\theta,\varphi) \right|^2 d\Omega} \tag{1}$$

As shown in Fig. 16(a), the ECC of antenna is less than 0.04 in the whole operating band according to the calculation formula of ECC. Diversity gain (DG) is another important performance index of the MIMO antennas. It refers to the difference in receiving level between diversity receiving and single receiving in a certain cumulative percentage of time. The greater the level difference is, the higher the diversity gain is, which indicates that the diversity improvement effect is better. Here is the formula for calculating the diversity gain:

$$DG = 10\sqrt{1 - ECC^2} \tag{2}$$

according to the formula, when ECC is smaller, diversity gain will be higher. As shown in Fig. 16(b), the DG of the antenna is approximately equal to 10 in the whole operating band.

To address the advantages of the proposed design, Table 2 tabulates the comparison results of 11 designs. It is seen that the proposed antenna has the advantages of compact size, wide operating band, high isolation, high peak gain, high efficiency, and low ECC value. It is worth mentioning that the bandwidth of the proposed design is the largest. In addition, the antenna efficiency within the whole operating band (165%) is better than 85%.

5. CONCLUSION

In this paper, a UWB-MIMO antenna based on the dual mode transmission line (DMTL) feeding has been proposed. Unlike the existing UWB-MIMO antenna, a new method of realizing ultra-wideband characteristics has been elaborated. By employing DMTL in a CPW feeding line, the impedance bandwidth can be enlarged a lot. Based on the DMTL feeding and U-shaped decoupling structure, the UWB-MIMO antenna possesses the characteristics of wide bandwidth of 2.4–25 GHz and high isolation of 20 dB in the whole working band. Moreover, the radiation efficiency of the antenna is above 85%; envelope correlation coefficient is less than 0.002; the diversity gain is about 10 dB, showing good MIMO performances.

REFERENCES

[1] Staderini, E., "UWB radars in medicine," *IEEE Aerospace and Electronic Systems Magazine*, Vol. 17, No. 1, 13–18, Jan. 2002.

[2] Zhang, J., P. V. Orlik, Z. Sahinoglu, A. F. Molisch, and P. Kinney, "UWB systems for wireless sensor networks," *Proceedings of The IEEE*, Vol. 97, No. 2, SI, 313–331, Feb. 2009.

[3] Alsath, M. G. N. and M. Kanagasabai, "Compact UWB monopole antenna for automotive communications," *IEEE Transactions on Antennas and Propagation*, Vol. 63, No. 9, 4204–4208, Sep. 2015.

[4] Ahmad, S., U. Ijaz, S. Naseer, A. Ghaffar, M. A. Qasim, F. Abrar, N. O. Parchin, C. H. See, and R. Abd-Alhameed, "A jug-shaped CPW-fed ultra-wideband printed monopole antenna for wireless communications networks," *Applied Sciences-basel*, Vol. 12, No. 2, Jan. 2022.

[5] Khan, M. S., S. A. Naqvi, A. Iftikhar, S. M. Asif, A. Fida, and R. M. Shubair, "A WLAN band-notched compact four element UWB MIMO antenna," *International Journal of RF and Microwave Computer-aided Engineering*, Vol. 30, No. 9, Sep. 2020.

[6] Huang, J., G. Dong, J. Cai, H. Li, and G. Liu, "A quad-port dual-band MIMO antenna array for 5G smartphone applications," *Electronics*, Vol. 10, No. 5, 542, 2021.

[7] Li, R., Z. Mo, H. Sun, X. Sun, and G. Du, "A low-profile and high-isolated MIMO antenna for 5G mobile terminal," *Micromachines*, Vol. 11, No. 4, Apr. 2020.

[8] Sehrai, D. A., M. Abdullah, A. Altaf, S. H. Kiani, F. Muhammad, M. Tufail, M. Irfan, A. Glowacz, and S. Rahman, "A novel high gain wideband MIMO antenna for 5G millimeter wave applications," *Electronics*, Vol. 9, No. 6, 1031, 2020.

[9] Radhi, A. H., R. Nilavalan, Y. Wang, H. Al-Raweshidy, A. A. Eltokhy, and N. A. Aziz, "Mutual coupling reduction with a wideband planar decoupling structure for UWB-MIMO antennas," *International Journal of Microwave and Wireless Technologies*,

Vol. 10, No. 10, 1143–1154, 2018.

[10] Rekha, V. S. D., P. Pardhasaradhi, B. T. P. Madhav, and Y. U. Devi, "Dual band notched orthogonal 4-element MIMO antenna with isolation for UWB applications," *IEEE Access*, Vol. 8, 145 871–145 880, 2020.

[11] Khan, M. S., A. Iftikhar, R. M. Shubair, A. D. Capobianco, B. D. Braaten, and D. E. Anagnostou, "A four element, planar, compact UWB MIMO antenna with WLAN band rejection capabilities," *Microwave and Optical Technology Letters*, Vol. 62, No. 10, 3124–3131, Oct. 2020.

[12] Wu, W., B. Yuan, and A. Wu, "A quad-element UWB-MIMO antenna with band-notch and reduced mutual coupling based on EBG structures," *International Journal of Antennas and Propagation*, Vol. 2018, 2018.

[13] Desai, A., J. Kulkarni, M. M. Kamruzzaman, S. Hubalovsky, H.-T. Hsu, and A. A. Ibrahim, "Interconnected CPW fed flexible 4-port MIMO antenna for UWB, X, and Ku band applications," *IEEE Access*, Vol. 10, 57 641–57 654, 2022.

[14] Ahmad, S., S. Khan, B. Manzoor, M. Soruri, M. Alibakhshikenari, M. Dalarsson, and F. Falcone, "A compact CPW-fed ultra-wideband multi-input-multi-output (MIMO) antenna for wireless communication networks," *IEEE Access*, Vol. 10, 25 278–25 289, 2022.

[15] Sharma, P., R. N. Tiwari, P. Singh, P. Kumar, and B. K. Kanaujia, "MIMO antennas: design approaches, techniques and applications," *Sensors*, Vol. 22, No. 20, Oct. 2022.

[16] Ravi, K. C. and J. Kumar, "Miniaturized parasitic loaded high-isolation MIMO antenna for 5G applications," *Sensors*, Vol. 22, No. 19, Oct. 2022.

[17] Nej, S., A. Ghosh, S. Ahmad, A. Ghaffar, and M. Hussein, "Compact quad band MIMO antenna design with enhanced gain for wireless communications," *Sensors*, Vol. 22, No. 19, Oct. 2022.

[18] Wen, C. P., "Coplanar waveguide: A surface strip transmission line suitable for nonreciprocal gyromagnetic device applications," *IEEE Transactions on Microwave Theory and Techniques*, Vol. MT17, No. 12, 1087–1090, 1969.

[19] Ma, K. P., Y. Qian, and T. Itoh, "Analysis and applications of a new CPW-slotline transition," *IEEE Transactions on Microwave Theory and Techniques*, Vol. 47, No. 4, 426–432, Apr. 1999.

[20] Wu, M.-D., S.-M. Deng, R.-B. Wu, and P. Hsu, "Full-wave characterization of the mode conversion in a coplanar waveguide right-angled bend," *IEEE Transactions on Microwave Theory and Techniques*, Vol. 43, No. 11, 2532–2538, 1995.

[21] Zuo, M., J. Ren, and Y. Z. Yin, "Dual-band antenna with large frequency ratio based on dual-mode transmission line," *IEEE Antennas and Wireless Propagation Letters*, Vol. 20, No. 10, 2068–2072, Oct. 2021.

[22] Dastranj, A., "Low-profile ultra-wideband polarisation diversity antenna with high isolation," *IET Microwaves Antennas & Propagation*, Vol. 11, No. 10, 1363–1368, Aug. 2017.

[23] Rajkumar, S., A. A. Amala, and K. T. Selvan, "Isolation improvement of UWB MIMO antenna utilising molecule fractal structure," *Electronics Letters*, Vol. 55, No. 10, 576–578, May 2019.

[24] Gomez-Villanueva, R. and H. Jardon-Aguilar, "Compact UWB uniplanar four-port MIMO antenna array with rejecting band," *IEEE Antennas and Wireless Propagation Letters*, Vol. 18, No. 12, 2543–2547, Dec. 2019.

[25] Raheja, D. K., B. K. Kanaujia, and S. Kumar, "Compact four-port MIMO antenna on slotted-edge substrate with dual-band rejection characteristics," *International Journal of RF and Microwave Computer-aided Engineering*, Vol. 29, No. 7, Jul. 2019.

[26] Sharawi, M. S., "Current misuses and future prospects for printed multiple-input, multiple-output antenna systems," *IEEE Antennas and Propagation Magazine*, Vol. 59, No. 2, 162–170, Apr. 2017.